Detection and Imaging of Oxygen-Centered Free Radicals with Low-Frequency Electron Paramagnetic Resonance and Signal-Enhancing Deuterium-Containing Spin Traps†

Howard J. Halpern,*,‡,§ Sovitj Pou,‖ Miroslav Peric,§ Cheng Yu,§ Eugene Barth,‡ and Gerald M. Rosen‖,⊥

Contribution from the Department of Radiation and Cellular Oncology, University of Chicago, and Michael Reese/University of Chicago Center for Radiation Therapy, Chicago, Illinois 60637, Department of Pharmacology and Toxicology, University of Maryland School of Pharmacy, Baltimore, Maryland 21201, and Veterans Administration Medical Center, Baltimore, Maryland 21218. *Received February 17, 1992*

Abstract: We have identified and imaged oxygen-centered free radicals with low-frequency electron paramagnetic resonance (EPR) spectroscopy and deuterium-containing spin traps to probe the feasibility of spin trapping deep in large (~10 cm), heterogeneous aqueous/hydrophobic (e.g., biologic) systems. Spectra at 250 MHz from spin trapping superoxide and hydroxyl radicals in aqueous solutions of deuterated analogs of DMPO (5,5-dimethyl-1-pyrroline-1-oxyl) were obtained, and the superoxide measurements were compared with those at X-band. Modification of X-band spectral line positions occurs due to the breakdown of the high-field approximation. Solution of the Breit-Rabi equations governing low-field measurements reproduces most of the observed line position changes. Sensitivity is found to scale with (frequency)^N, with $N \sim 1.6$ largely compensated for by the increase in sample volume. A two-dimensional spectral-spatial image of a phantom filled with heterogeneous concentrations of spin trap and subjected to γ radiation from ^{60}Co is presented.

Introduction

Spin trapping[1-5] is the current method of choice for the detection, characterization, and localization of free radicals in cells, isolated organs, and whole animals.[6-12] Until recently, it has been difficult to identify free radicals in any sophisticated biological model other than isolated cells or perfusates.[13,14] However, advances in low-frequency electron paramagnetic resonance (EPR) spectroscopy[15-25] provide the potential for identifying and localizing free radicals in situ and in vivo. With low-frequency EPR spectroscopy, one can measure free radicals in heterogeneous aqueous/lipid tissues at depths on the order of 10 cm rather than the millimeter depths accessible to conventional EPR spectroscopy. However, operating at low frequency involves a sacrifice in overall sensitivity as compared with measurements at higher frequencies.[15] The question to which this study is devoted is the feasibility of spin trapping at frequencies sufficiently low for full sensitivity in the heterogeneous aqueous/lipid samples of animal tissue. This is a precondition for true spin trapping in vivo.

To overcome the low-frequency sensitivity limitation, a chemical solution is proposed: the synthesis of a family a deuterium- and ^{15}N-containing 5,5-dimethyl-1-pyrroline-N-oxyls (DMPO, I).[26] These compounds have been shown to increase the sensitivity of the spin-trapping method significantly.[26] In this paper, we report the ability to spin trap both superoxide and hydroxyl radicals at very low frequency by using several different deuterium-labeled DMPOs. The sensitivity at low frequency is compared with that at conventional X-band frequencies (9.5 GHz). The spectral changes at low frequency as compared with X-band are modeled by consideration of the breakdown of the high-field approximation. A two-dimensional spectral-spatial image of the spin-trapped adduct DMPO-d_{11}-OH (IX) (2-hydroxy-5,5-di[$^2H_3$]methyl-[2,3,3,4,4-$^2H_5$]pyrrolidine-1-oxyl) is shown.

Experimental Section

Materials. Diethylenetriaminepentaacetic acid (DTPA), superoxide dismutase, xanthine, and ferricytochrome *c* (type VI) were purchased from Sigma Chemical Company (St. Louis, MO). Sodium phosphate monobasic and dibasic were purchased from J. T. Baker, Inc. (Phillips-

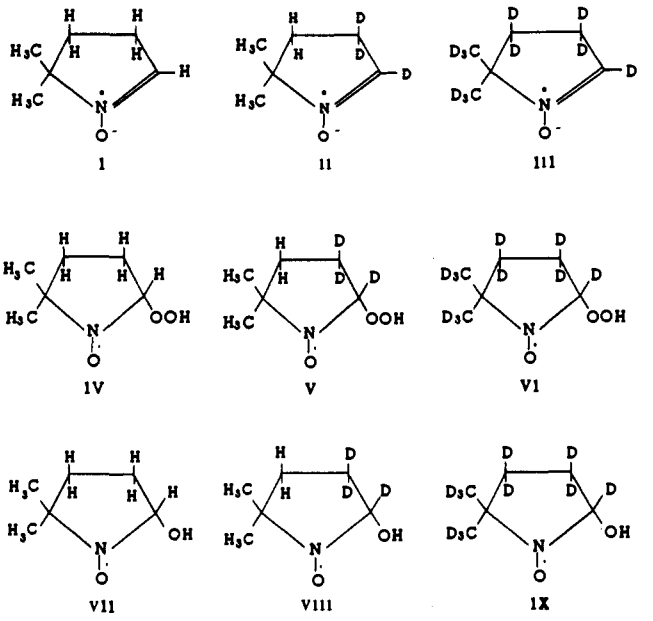

* To whom correspondence should be addressed.

† Preliminary work was presented at the 5th Biennial Meeting of the International Society for Free Radical Research, Pasadena, CA, November 1990; the 8th International Congress on Radiation Research, Toronto, Ontario, Canada, July 1991; and the 15th International EPR Symposium of the Rocky Mountain Conference on Applied Spectroscopy, Denver, CO, August 1991.

‡ University of Chicago.
§ Michael Reese/University of Chicago Center for Radiation Therapy.
‖ University of Maryland School of Pharmacy.
⊥ Veterans Administration Medical Center.

(1) Janzen, E. G. *Acc. Chem. Res.* **1971**, *4*, 31.
(2) Finkelstein, E.; Rosen, G. M.; Rauckman, E. J. *Arch. Biochem. Biophys.* **1980**, *200*, 1.
(3) Janzen, E. G. In *Free Radicals in Biology, A critical review of spin trapping in biological systems*; Pryor, W. A., Ed.; Academic Press: New York, 1980; Vol. 4, pp 116.
(4) Pou, S.; Hassett, D. J.; Britigan, B. E.; Cohen, M. S.; Rosen, G. M. *Anal. Biochem.* **1989**, *177*, 1.
(5) Janzen, E. G.; Haire, D. L. Two decades of spin trapping. In *Advances in Free Radical Chemistry*; Tanner, D., Ed.; JAI Press: Greenwich, CT, 1990; Vol. 1, pp 253.
(6) Granger, D. N.; Rutili, G.; McCord, J. M. *Gastroenterology* **1981**, *81*, 22.
(7) Gurtner, G. H.; Michael, J. R.; Farukh, I. S.; Sciuto, A. M.; Adkinson, N. F. *J. Appl. Physiol.* **1985**, *59*, 953.
(8) Palmer, R. M. J.; Ferrige, A. G.; Moncada, S. *Nature* **1987**, *327*, 524.
(9) Azuma, H.; Ishikawa, M.; Sekizaki, S. *Br. J. Pharmacol.* **1986**, *88*, 411.
(10) Furlong, B.; Henderson, A. H.; Lewis, M. J.; Smith, J. A. *Br. J. Pharmacol.* **1987**, *90*, 687.
(11) Radomski, M. W.; Palmer, R. J. M.; Moncada, S. *Br. J. Pharmacol.* **1987**, *92*, 181.

0002-7863/93/1515-218$04.00/0

Table I. Modulation Field Amplitudes (in G) for the Various Spectra from the Indicated Spin-Trapped Adducts (Taken at the Frequencies Indicated) Shown in Figures 2–4[a]

spin-trapped adduct	frequency (MHz)	modulation amplitude (G)	simulation line width (G)
DMPO-OOH	9500	1.6	1.6
DMPO-d_3-OOH	9500	1.0	1.1
DMPO-d_{11}-OOH	9500	0.2	0.4
DMPO-OOH	250	1.5	1.5
DMPO-d_3-OOH	250	0.5	1.0
DMPO-d_{11}-OOH	250	0.3	0.4
DMPO-OH	250	1.5	1.5
DMPO-d_3-OH	250	1.0	1.0
DMPO-d_{11}-OH	250	0.3	0.7

[a] Also listed are the line widths found by simulation to reproduce the gross features of the EPR spectrum most accurately.

burg, NJ). Buffers were passed through a column loaded with Chelex 100 from Bio-Rad (Richmond, CA). Xanthine oxidase was obtained from Calbiochem (La Jolla, CA). Catalase was obtained from Boehringer Mannheim (Indianapolis, IN). The spin traps, DMPO (I), DPMO-d_3 (II) (5,5-dimethyl[2,3,3-$^2H_3$]-1-pyrroline-1-oxyl), and DMPO-d_{11} (III) (5,5-di[$^2H_3$]methyl[2,3,3,4,4-$^2H_5$]-1-pyrroline-1-oxyl), were synthesized according to procedures outlined by Bonnett et al.[27] and Pou et al.[26]

Instrumental Conditions. A low-frequency EPR spectrometer previously described[15] was operated at 250 MHz. At this frequency, the skin depth (37% sensitivity) is approximately 6 cm of tissue depth. The spectrometer consists of a lumped circuit parallel inductance and capacitance resonator, in which the single-turn inductance is the sample holder. The capacitive coupling is adjustable electronically. This allows sample and microphonic-induced variations in the coupling to be corrected for variations of frequencies up to several hundred Hz. The characteristics of the resonator are such that the radiofrequency magnetic field (B_1) with a radiofrequency power of 100 mW, at a loaded Q (quality factor) of approximately 35, produced by a 10-mL buffer solution sample, is 0.1 G. This is 40% lower than that of the X-band TE_{102} cavity at 20-mW input power (calculated to the approximately 0.14 G). The modulation frequency was 5.12 kHz. Modulation field amplitudes were adjusted to match the anticipated spectral line width. The line width varies with the extent of deuteration. The modulation amplitudes and the simulation line widths are listed in Table I. Data aquisition was accomplished under the control of a microcomputer. Spectra were obtained with 256 points per scan, 15 scans per spectrum. The time constant and point aquisition time were 0.1 s, giving a spectral acquisition time of 6.5 min. The largest spectral window currently conveniently available with the low-frequency spectrometer is 42 G. Thus, spectra obtained from the reaction of DMPO (I) with either superoxide or hydroxyl radical taken at 250 MHz are truncated just before the upfield line.

Spectra obtained at X-band were recorded with a Varian E-109 spectrometer with a TE_{102} cavity and at a power of 20 mW. Spectra were obtained in a single 8-min scan with a time constant of 1 s. X-band spectra were taken with varied modulation amplitudes similar to those at low frequency. These amplitudes are indicated in Table I. Spectrometer gains are given in the figure captions. The modulation frequency was 100 KHz. We estimate that the volume to which the spectrometer is sensitive is 0.08 mL.

Table II. Hyperfine Couplings A_N[a]

compound	A_N (G)	$A_{H(D)\beta}$ (G)	$A_{H(D)\gamma}$ (G)
DMPO-OOH	14.3	11.4	1.25
DMPO-d_3-OOH	14.3	1.76	0.19
DMPO-d_{11}-OOH	14.3	1.76	0.19
DMPO-OH	14.8	14.8	
DMPO-d_3-OH	14.8	2.26	
DMPO-d_{11}-OH	14.8	2.26	

[a] N refers to the coupling of the nucleus to the nitroxide electron. Couplings were used as the splittings at X-band or as input to the Breit–Rabi equations (see Supplementary Material) in the spectral simulation for the various deuterated species of both the superoxide spin-trapped adduct and the hydroxyl spin-trapped adduct of DMPO.

Superoxide Measurement and Spin Trapping. Superoxide production was measured as the superoxide dismutase-inhibitable reduction of ferricytochrome c (80 μM) and monitored spectrophotometrically at 550 nm, with an extinction coefficient of 21 mM^{-1} cm^{-1} as previously described.[28] Superoxide was generated by the addition of xanthine oxidase to a 50 mM aqueous phosphate buffer solution, pH 7.8, containing xanthine (400 μM) and 1 mM DTPA. Xanthine oxidase was added at a concentration that gave a superoxide flux of 10 μM/min. For superoxide spin-trapping experiments, DMPO (I), DMPO-d_3 (II), or DMPO-d_{11} (III) at a concentration of 0.1 M was substituted for cytochrome c as described above. For X-band measurements, reaction mixtures were transferred to a flat EPR quartz cell and fitted into the cavity of the EPR spectrometer. Spectra were recorded at 25 °C. For low-frequency measurements, reactants were mixed to a 10-mL volume in a polyethylene vial and placed in the 17-mL resonator of the 250-MHz spectrometer at 27 °C. Superoxide spin adduct spectral aquisition was begun 2 min after the reaction commenced.

Spin-Trapping Hydroxyl Radical and Imaging of Hydroxyl Radical Spin-Trap Adduct. Hydroxyl radical was produced by exposure of an air-equilibrated sample of 50 mM phosphate buffer, pH 7.8, plus 1 mM DTPA (together referred to as buffer), which contained spin trap at a concentration of 0.1 M, to radiation from ^{60}Co in a Gammacell irradiator at a dose rate of either 10^4 or 3×10^3 Gy/h. At these dose rates, the maximum time of irradiation was 10 min; most of the irradiations took less than 1 min. Hydroxyl adduct spectral aquisition was begun a minimum of 10 min after the irradiation was completed. The time elapsed between the end of irradiation and the beginning of the spectral measurement averaged 14.6 min. The stability and signal intensity of the hydroxyl spin-trap adduct allowed the imaging of a buffer-filled phantom shown in Figure 6. The phantom was divided into three axially disposed compartments with center-to-center distances of approximately 10 mm. The end disks were filled with buffer to which DMPO-d_{11} (III) (0.1 M) was added and were exposed as air-equilibrated solutions to 920 Gy of ^{60}Co γ radiation. The center disk remained empty. Beginning approximately 15 min after the end of the irradiation, two-dimensional spectral-spatial images[29] (one spectral dimension, one spatial dimension along the axis of the cylindrical disks) were obtained with the use of continuous-wave spectra from samples subjected to sequences of fixed gradients referred to as projections. Thirty-two projections were generated in 17 min by splaying the main-field coils to give a maximum (single) gradient of 3 G/cm as previously described.[15] Images were reconstructed by means of the back-projection reconstruction algorithm of Hayner[30] for incomplete angular coverage. The code for this has kindly been provided by S. Eaton and G. Eaton and modified by us for our particular use. This code[29,30] has been described previously and allows the treatment of "missing" lines and sample extent due to gradient and scan limitations.

Spectral Simulation. Optimum models of the 9.5-GHz spectra were made by adjustment of the spectral width. Where it appeared necessary to reproduce the gross features of the spectra, small variations (by no more than 3%) were introduced in the 9.5-GHz splittings from those quoted in the literature.[31,32] For DMPO spin-trap adducts, only β

(12) Sneddon, J. M.; Vane, J. R. *Proc. Natl. Acad. Sci. U.S.A.* **1988**, *85*, 2800
(13) Poyer, J. L.; McCay, P. B.; Lai, E. K.; Janzen, E. G.; Davis, E. R. *Biochem. Biophys. Res. Commun.* **1980**, *94*, 1154.
(14) Knecht, K. T.; Mason, R. P. *Drug Metab. Dispos.* **1991**, *19*, 325.
(15) Halpern, H. J.; Spencer, D. P.; VanPolen, J.; Bowman, M. K.; Nelson, A. C.; Dowey, E. M.; Teicher, B. A. *Rev. Sci. Instrum.* **1989**, *60*, 1040.
(16) Zavoisky, E. *J. Phys. (Moscow)* **1945**, *9*, 245.
(17) Duncan, W.; Schneider, E. E. *J. Sci. Instrum.* **1965**, *42*, 395.
(18) Hill, M. J.; Wyard, S. J. *J. Sci. Instrum.* **1967**, *44*, 433.
(19) Decorps, M.; Fric, C. *J. Phys. E* **1971**, *5*, 337.
(20) Nishikawa, H.; Fujii, H.; Berliner, L. J. *J. Magn. Reson.* **1985**, *62*, 79.
(21) Zweier, J. L.; Kuppusamy, P. *Proc. Natl. Acad. Sci. U.S.A.* **1988**, *85*, 5703.
(22) Froncisz, W.; Oles, T.; Hyde, J. S. *J. Magn. Reson.* **1989**, *82*, 109.
(23) Bacic, G.; Nilges, M. J.; Magin, R. L.; Walczak, T.; Swartz, H. M. *Magn. Reson. Med.* **1989**, *10*, 266.
(24) Ishida, S.; Kumashiro, H.; Tsuchihashi, N.; Ogata, T.; Ono, M.; Kamada, H.; Yoshida, E. *Phys. Med. Biol.* **1989**, *34*, 1317.
(25) Alecci, M.; Colacicchi, S.; Indovina, P. L.; Momo, F.; Pavone, P.; Sotgiu, A. *Magn. Reson. Imaging* **1990**, *8*, 59.
(26) Pou, S.; Rosen, G. M.; Wu, Y.; Keana, J. F. W. *J. Org. Chem.* **1990**, *55*, 4438.
(27) Bonnett, R.; Brown, R. F. C.; Clark, V. M.; Sutherland, I. O.; Todd, A. *J. Chem. Soc.* **1956**, 2094.
(28) Kuthan, H.; Ullrich, V.; Estabrook, R. W. *Biochem. J.* **1982**, *203*, 551.
(29) Maltempo, M. M.; Eaton, S. S.; Eaton, G. E. *J. Magn. Reson.* **1988**, *77*, 75.
(30) Hayner, D. A.; Jenkins, W. K. *The missing cone problem in computer tomography, Advances in computer vision and image processing*; JAI Press: Greenwich, CT, 1984; Vol. 1, pp 83.

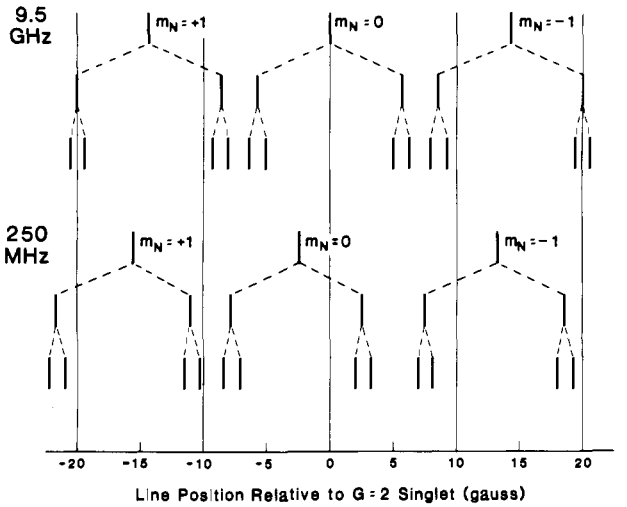

Figure 1. Stick diagram for spectrum of DMPO-OOH (IV) at 9.5 GHz and 250 MHz. The assignment of the splittings to the individual nuclear splittings is an adequate representation of the origin of the line positions at 9.5 GHz, where the high-field approximation is valid and where, to an excellent approximation, the energy eigenstates are unmixed eigenstates of the individual magnetic quantum numbers. This is *not* the case at 250 MHz, where the high-field approximation does not apply. The dotted lines relating the splittings induced by each nuclear coupling are retained for comparison with the 9.5-GHz diagram. Relative to the 9.5-GH spectrum, the 250-MHz spectrum demonstrates line shifts of between 3.1 and 1.1 G. These shifts substantially modify spectral simulations in which lines are of the order of 1 G in width and the largest splittings are roughly 20 G.

(position 2 of the heterocyclic ring) and γ (position 3 of the heterocycle ring) splittings were used. Other splittings were incorporated into the line width as unresolved. Fully and partially deuterated compounds were modeled with couplings reduced relative to those of the hydrogen-bearing counterparts by a factor of 6.51 (the ratio of the hydrogen to the deuterium gyromagnetic moment), and doublets were replaced by triplets. Unresolved γ splittings were treated as singlets of weight equal to the multiplicity. The couplings assumed for the spectral modeling of variously deuterated DMPO-OOHs (IV–VI) and DMPO-OHs (VII–IX) are listed in Table II.

The superoxide spin-trapped adduct of DMPO (IV) was modeled as consisting of 12 lines (nitrogen triplet and β- and γ-hydrogen doublets). Both the partially and the fully deuterated DMPO superoxide spin-trapped-adduct spectra—those of DMPO-d_3-OOH (V) and DMPO-d_{11}-OOH (VI)—were modeled as consisting of 27 lines (the product of the nitrogen triplet, and two deuterium triplets), although the γ deuterium triplet is unresolved, leaving 9 spectroscopically distinguished lines; the hydrogen/deuterium at position 4 and methyl-hydrogen/deuterium are considered to contribute to the unresolved line width. The spectrum of the hydroxyl spin-trapped adduct of DMPO (VII) was modeled as consisting of 6 resolved lines (nitrogen triplet and the β-hydrogen doublet) with the γ-, the δ- (position 4 on the heterocyclic ring), and the methyl-hydrogens unresolved. The spectrum of the hydroxyl spin-trapped adduct of the partially and fully deuterated DMPOs was modeled as consisting of 9 lines (nitrogen triplet and the β-deuterium triplet), with the nuclear splitting of the γ-deuterium and other hydrogens and/or deuterium unresolved.

Because of the breakdown of the high-field approximation at $B_0 = 90$ G (250 MHz), spectra at that field are expected to differ from those at $B_0 = 3300$ G. With the couplings of Table II, the Breit–Rabi spin Hamiltonian[33] was used to define the splittings at lower fields. This was solved exactly for DMPO-OOH and to second order for DMPO-OH, as

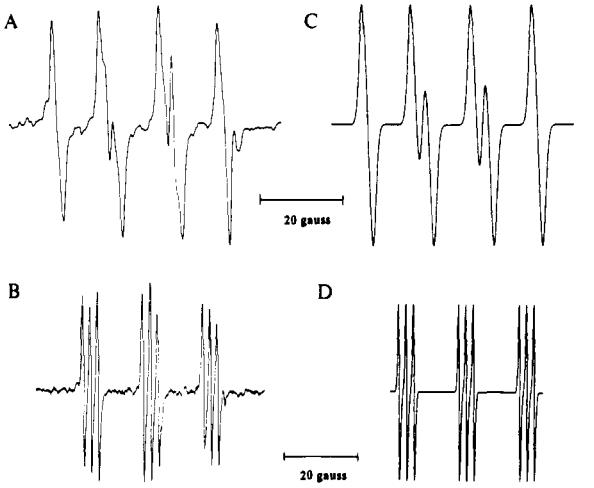

Figure 2. High-modulation amplitude spectra at 9.5 GHz (X-band) of the superoxide adducts of (A) DMPO (IV) and (B) DMPO-d_{11} (VI). Spectral conditions are as described in the text; modulation amplitudes are (A) 1.6 G and (B) 0.2 G, as in Table I, and spectrometer gains are (A) 5×10^4 and (B) 1×10^4. Spectral simulation of these spectra at 9.5 GHz is presented as follows: the superoxide adducts of (C) DMPO (IV) and (D) DMPO-d_{11} (VI). Coupling constants are (C) $A_N = 14.3$ G, $A_{H\beta} = 11.4$ G, and $A_{H\gamma} = 1.25$ G and (D) $A_N = 14.3$ G, $A_{D\beta} = 1.76$ G, and $A_{D\gamma} = 0.19$ G, as in Table II. The simulation spectral widths used are (C) 1.6 G and (D) 0.4 G, as in Table I (Gaussian line shape).

described in the Supplementary Material. It was accomplished with the use of code kindly provided by S. Marshall of the Department of Physics, Michigan Technological University, Houghton, MI.

A stick diagram is shown in Figure 1, comparing the line positions of DMPO-OOH (IV) relative to the $g = 2$ position at 9.5 GHz and 250 MHz. At 250 MHz, the nitrogen splittings are represented with zero hydrogen coupling; the next line involves the result from turning on the β-hydrogen coupling; the actual position is that calculated from the eigenvalues of the full 24 × 24 Hamiltonian matrix equation. The positions of the corresponding lines at 250 MHz vary from those at 9.5 GHz by 1.1–3.1 G.

Results

Measurement of Spin Trapping of Superoxide. When xanthine oxidase was placed into a solution containing xanthine, DPTA (0.1 mM), and DMPO (I), DMPO-d_3 (II), or DMPO-d_{11} (III) in the X-band EPR spectrometer, spectra (Figure 2) were recorded which were inhibited by SOD (30 units/mL) but not by catalase (300 units/mL). On the basis of spectral simulation (Figure 2) and literature references,[26,31,32] these spectra are assigned to the corresponding spin-trapped adducts DMPO-OOH (IV) (Figure 2A,C) and DMPO-d_{11}-OOH (VI) (2-hydroperoxy-5,5-di[$^2H_3$]-methyl[2,3,3,4,4-$^2H_5$]pyrrolidine-1-oxyl) (Figure 2B,D). Spectra and simulation for DMPO-d_3-OOH (V) (2-hydroperoxy-5,5-dimethyl[2,3,3-$^2H_3$]pyrrolidine-1-oxyl) are shown in the Supplementary Material, Figure 1S. Previous X-band measurements at a constant low modulation field,[26] 0.2 G, (see Supplementary Material Figure 1S) indicate that, as the spin trap is changed from DMPO (I) to DMPO-d_3 (II) to DMPO-d_{11} (III), the signal-to-noise ratio of the corresponding spin-trapped adduct increases by a factor of between 1.5 and 2 for each change. Simulations of these spectra (also presented in Supplementary Material, Figure 1S) demonstrate that two factors are responsible for the increase in signal height. The first is the collapse of the 1.25-G γ-H splitting to 0.19 G for the γ-D splitting, reducing the effective number of spectral lines from 12 in the case of DMPO-OOH (IV) to 9 for DMPO-d_3-OOH (V). The remainder of the increase is due to the lack of interference between the closely spaced lines, which otherwise causes a partial cancellation in the derivative spectral lines of DMPO-OOH (IV). For DMPO-d_{11}-OOH (VI), the further increase in spectral height is due to the reduction in spectral width from inhomogeneous broadening induced by the substitution of low-magnetic-coupling deuterium for hydrogen nuclear spins on the methyl groups bonded to the ring carbon at position 5 and the nuclear spins of hydrogen directly bonded to

(31) Finkelstein, E.; Rosen, G. M.; Raukman, E. J. *J. Am. Chem. Soc.* **1980**, *102*, 4994.

(32) Finkelstein, E.; Rosen, G. M.; Rauckman, E. J.; Paxton, J. *Mol. Pharmacol.* **1979**, *16*, 676.

(33) (a) Breit, G.; Rabi, I. I. *Phys. Rev.* **1931**, *38*, 2082. (b) Abragam, A. *Principles of Nuclear Magnetism*; Oxford University Press: Oxford, England, 1961; p 341. (c) Wertz, J. E.; Bolton, J. R. *Electron Spin Resonance: Elementary Theory and Practical Applications*; Chapman and Hall: New York, 1986; pp 436. (d) Pake, G. E.; Estle, T. L. *The Physical Principles of Electron Paramagnetic Resonance*, 2nd ed.; W. A. Benjamin: Reading, MA, 1973; pp 144, 293.

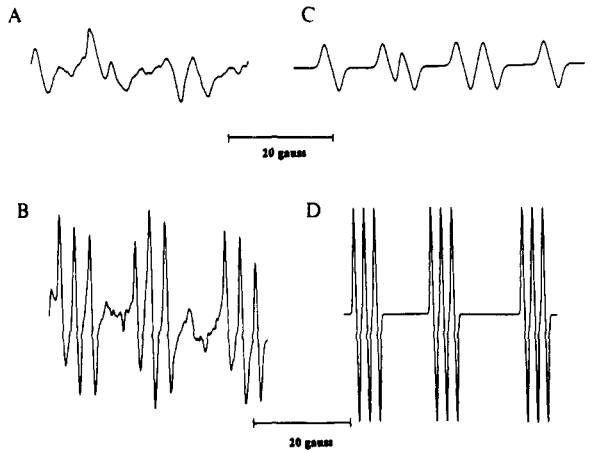

Figure 3. Spectra at 250 MHz of the superoxide adduct of (A) DMPO (IV) and (B) DMPO-d_{11} (VI). Spectral conditions are as described in the text. Modulation amplitudes are (A) 1.5 G and (B) 0.3 G, as in Table I. The spectrum in Figure 3A is incomplete in that the spectral window of the spectrometer is temporarily limited to 42 G. Spectral simulation at 250 MHz of the superoxide adduct is presented for (C) DMPO (IV) and (D) DMPO-d_{11} (VI). The hyperfine couplings are (C) A_N = 14.3 G, $A_{H\beta}$ = 11.4 G, and $A_{H\gamma}$ = 1.25 G and (D) A_N = 14.3 G, $A_{D\beta}$ = 1.76 G, and $A_{D\gamma}$ = 0.19 G, as in Table II. The hyperfine-splitting patterns are substantially different from the couplings due to the breakdown of the high-field approximation, as discussed in the text. The simulation spectral widths (Gaussian line shape) are 1.5 and 0.4 G, as in Table I.

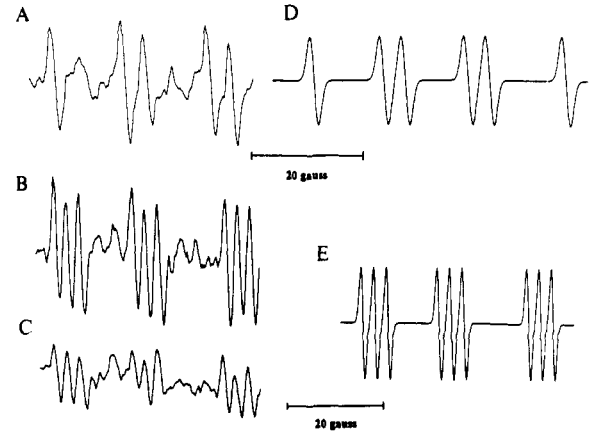

Figure 4. Spectra at 250 MHz of the hydroxyl adduct of (A) DMPO (VII) and (B and C) DMPO-d_3 (VIII). B and C differ in that hydroxyl radical is produced by 50-Gy γ radiation in B and by 15-Gy γ radiation in C. Spectral conditions are as indicated in the text. Modulation amplitudes are (A) 1.5 G and (B and C) 1.0 G, as in Table I. Spectral simulations are presented for the hydroxyl adducts of (D) DMPO (VII) and (E) DMPO-d_3 (VIII). Coupling constants are (D) A_N = 14.8 G and $A_{H\beta}$ = 14.8 G and (E) A_N = 14.8 G and $A_{D\beta}$ = 2.26 G, as in Table II. As in Figure 3, these couplings do not correspond to the splittings, because of the breakdown of the high-field approximation and the need to calculate the splittings from the eigenvalues of the full hyperfine interaction (Breit–Rabi Hamiltonian). The spectral widths used in the simulation (Gaussian line shape) are (D) 1.5 G and (E) 1.0 G, as in Table I.

the carbon at position 4 on the pyrrolidine-1-oxyl ring.

For comparison with the signal-to-noise ratio obtained at low frequency, the X-band measurements of the superoxide adduct of the variously deuterated analogs of DMPO (I) were repeated with higher modulation amplitude to increase the signal-to-noise ratio (sensitivity), consistent with spectral recognition. Modulation amplitudes were chosen to approximate the expected line width. Modulation amplitudes and the spectral widths used in simulation are shown in Table I, and the spectra are shown in Figure 2. These various modulation amplitudes, which are roughly signal-optimized, tend to reduce the signal-to-noise ratio differences between the compounds at the expense of spectral specificity for the spin-trapped adduct. The noise is defined to be variation in the wings of the spectrum and/or between spectral lines. The signal-to-noise ratio (peak-to-peak signal/noise standard deviation) for each spectrum in Figure 2 is approximately 150:1.

The DMPO-OOH (IV) spectrum, obtained with the low-frequency EPR spectrometer at 250 MHz, is shown in Figure 3A. Again, this assignment is based on the finding that the spectrum was inhibited by SOD (30 units/mL) but not by catalase (300 units/mL). The last line is truncated because of limitations on the spectrometer field window. The line positions of the spectrum, relative to the $g = 2$ magnetic field, when the exact Breit–Rabi Hamiltonian is used, are listed in Table 1S of the Supplementary Material. The simulation of this spectrum is shown in Figure 3C; with the spectral parameters of Tables I and II, the simulation reproduces the salient features of the spectrum. The signal-to-noise ratio is diminished by a factor of ~4 with respect to that of the X-band measurements.

The EPR spectrum of the superoxide adduct of DMPO-d_{11} (VI), measured at 250 MHz, is shown in Figure 3B. The EPR spectrum at 250 MHz of the superoxide adduct of DMPO-d_3 (V) and its simulation are shown in Supplementary Material Figure 2S. The line positions of the spectrum for the exact Breit–Rabi Hamiltonian are listed in Supplementary Material Table 2S. Spectral simulation of DMPO-d_{11}-OOH (VI) is shown in Figure 3D. For DMPO-d_{11}-OOH (VI) (three experiments, nine spectra), there is a consistent discrepancy of approximately 60% between the β-hydrogen splitting indicated by the simulation and that found in the spectrum. The loss of signal-to-noise ratio of these spectra compared with those from the X-band measurements is approximately a factor of 4.

Measurements of Spin-Trapping Hydroxyl at 250 MHz with Spectral Simulation. Spectra at 250 MHz of the hydroxyl spin-trapping adducts of DMPO (I) and DMPO-d_3 (II), yielding DMPO-OH (VII) and DMPO-d_3-OH (VIII) (2-hydroxy-5,5-dimethyl[2,3,3-$^2H_3$]pyrrolidine-1-oxyl) are presented in Figure 4A,C. The assignment of hydroxyl adduct is based on the production method, previous studies with radiolysis[34] producing the spin-trapped adduct characteristic of that of hydroxyl produced by other methods,[31,32,35,36] and the spectral modeling agreement seen in Figure 4D,E. Spectra are shown in Figure 4A,B from hydroxyl spin-trapped adducts at 50-Gy exposure with DMPO (I) and DMPO-d_3 (II) used, respectively. Figure 4C shows the spectrum of DMPO-d_3-OH (VIII) at 15-Gy exposure. Figure 3S of the Supplementary Material shows a spectrum of DMPO-d_{11}-OH (IX) at 50-Gy with a somewhat better signal-to-noise ratio.

The time dependence of the spin-trapped adduct is biphasic, with an initial phase of a half-life of approximately 30 min, consistent with prior measurements.[34] The dose dependence of the signal height from DMPO (I) exposed to 10^4 Gy/h ^{60}Co γ radiation yielding DMPO-OH (VII) at various times after irradiation is shown in Figure 5. The onset of saturation is time-dependent, but saturation is essentially complete at a dose of 300 Gy. These results are consistent with prior quantitative measurements.[34] The half-life of 30 min allows the delays between radiation and spectral aquisition referred to in the Experimental Section. The positions of the lines as derived from the solutions of the Breit–Rabi Hamiltonian[33] equations are available in Supplementary Material Table 3S and 4S. At X-band frequencies, the low-field line of DMPO-d_3-OOH (V) and DMPO-d_{11}-OOH (VI) differs from that of DMPO-d_3-OH (VIII) and DMPO-d_{11}-OH (IX) by 1.1 G. At 250 MHz, this difference between the low-field line positions is seen to be virtually identical. DMPO-d_{11}-OOH (VI) and DMPO-d_{11}-OH (IX) spectra are measured optimally at low-modulation fields (0.2–0.3 G) yielding narrow (0.3–0.5 G) lines. This allows spectral distinction between these two spin-trapped adducts which is at least as sharp at 250 mHz

(34) Carmichael, A. J.; Makino, K.; Riesz, P. *Radiat. Res.* **1984**, *100*, 222.
(35) Harbour, J. R.; Chow, V.; Bolton, J. R. *Can. J. Chem.* **1974**, *52*, 3549.
(36) Janzen, E. G.; Wang, Y. Y.; Shetty, R. V. *J. Am. Chem. Soc.* **1978**, *100*, 2923.

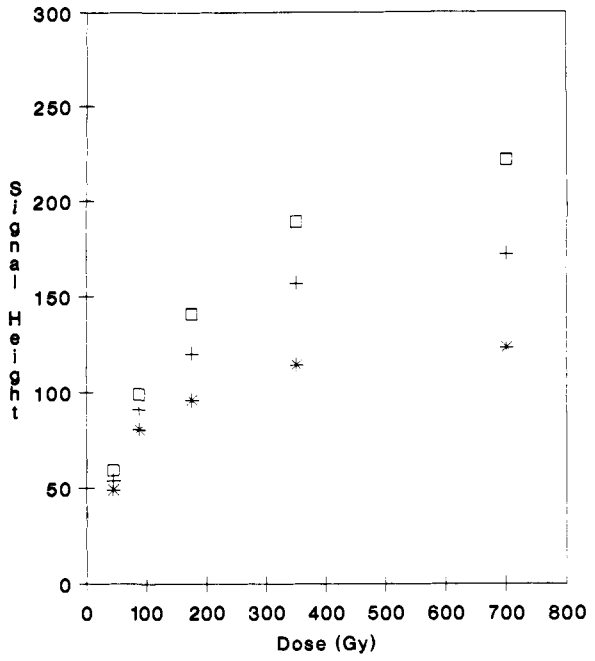

Figure 5. Spectral signal height of DMPO-OH (VII) versus the γ radiation dose to which a sample of DMPO has been exposed. Spectral height is defined as the peak-to-trough height variation of the average of five spectral lines shown in Figure 4A. Spectral conditions are those indicated for Figure 4A. The symbols indicate spectral height measured at different times after radiation is completed: □, 20 min after completion of the radiation; +, 30 min after completion of the radiation; ✱, 50 min after completion of the radiation. The relative uncertainties of the spectral height measurements are ±5% based on three separate measurements.

as that done with spin-trapping adducts of DMPO at 9.5 GH.

Imaging of the Spin Trapping of Hydroxyl in a Phantom. The two-dimensional spectral-spatial image derived from the phantom (shown in Figure 6) with its small compartment filled with 0.5 mL of DMPO-d_{11} (III) (0.1 M) in buffer, its central compartment empty, and its last compartment filled with 2.5 mL of DMPO-d_{11} (III) (0.1 M) in buffer and exposed to 920-Gy ^{60}Co γ radiation is shown in Figure 6. Given the response curve of Figure 5, this is equivalent to a dose of approximately 300 Gy. The compartments are clearly distinguished along the spatial axis. The spectral dimension, whose interval contains only the central triplet, also clearly shows the expected spectrum.

Relative Sensitivity of Measurements at Low Frequency. The use of buffered solutions for the measurement of the spin trapping of superoxide lowered the Q (to which the signal is proportional) to a value of 35, lower than that of an animal residing in the spectrometer resonator (Q = 50). Given the animal-induced noise, these conditions approximate those with a living animal present or those involving an isolated perfused organ.[37] The sensitive volume differs by a factor of approximately 125 between the X-band and 250-MHz spectrometers. With a sensitivity that scales as (frequency)^N where N = 1, a decrease by a factor of 40 in the sensitivity, combined with the volume advantage of the 250-MHz spectrometer corrected for the 40% higher X-band B_1, should yield a net increase in sensitivity at 250 MHz by a factor of 2. In fact, the sensitivity of the low-frequency spectrometer is a factor of 4 worse, corresponding to $N \sim 1.6$. The likely source of this extra factor of 8 in the decrease in sensitivity is the failure of the lock-in amplifier to fully protect the signal from noise due to mechanically modulated ground currents at the modulation frequency. This noise source is currently being addressed. An increase in sensitivity by a factor of 4–10 would also allow quantitative measurement of the production of hydroxyl radicals

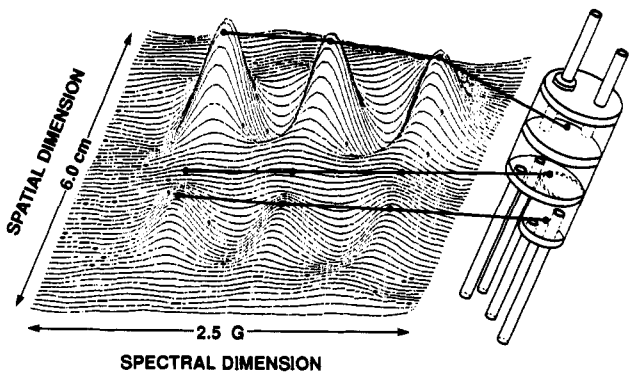

Figure 6. Two-dimensional spectral-spatial image of the phantom shown on the right side of the figure. The compartments nearest the bottom and top of the figure are filled with 0.1 M DMPO-d_{11} (III) in buffer and exposed to 920-Gy ^{60}Co γ radiation. Spectrometer conditions include a radiofrequency of 250 MHz, RF power of 100 mW, modulation frequency of 5.12 KHz, modulation amplitude of 330 mG, lock-in time constant of 0.1 s, data sampling rate of 10 points/s, 64 points per scan, 5 scans per spectrum. The image was reconstructed from 32 spectra at various field gradients, all obtained in 17 min. The direction across the page is the spectral dimension. The spatial dimension is seen into the page. The phantom consists of disks in tandem whose centers are spaced 10-mm apart. The lines indicate the spatial region of the image associated with each compartment. The spectral interval corresponds to the central triplet of DMPO-d_{11}-OH (IX).

at doses (~2–4 Gy) that approach those used clinically.[38]

Discussion

The difficulty in the detection and characterization of free radicals that evolve deep in heterogeneous polar/nonpolar solvent systems—e.g., living tissues—is, in principle, solved with low-frequency EPR spectroscopy. At 250 MHz, this technique can be used for measurements in such samples at depths of many centimeters. However, with the change of frequency from the more conventional 9.5 GHz to 250 MHz, one would anticipate a significant decrease in sensitivity, as earlier studies have shown.[15,37,39] A chemical approach to this limitation involves the synthesis of deuterium and ^{15}N-labeled spin traps.[26] These measurements lend credence to the principle of this solution.

This work demonstrates that both superoxide and hydroxyl radicals can be detected with spin trapping and EPR spectroscopy at 250 MHz. Signals are simplified and the signal-to-noise ratio is increased when the deuterium-containing spin traps DMPO-d_3 (II) and DMPO-d_{11} (III) are used. Spin-trapped adduct specificity, however, is not compromised. In the case of hydroxyl radicals produced radiolytically, low-frequency spin trapping allows detection at doses low enough to be of radiobiological significance and that approach individual fraction doses used in the treatment of cancer. The interpretation of spectra from spin-trapping experiments at low frequency requires due attention to the effects of the breakdown of the low-field approximation. Most of the shifts in the line positions at 250 MHz from those at 9.5 GHz are shown to be the consequence of the off-diagonal terms in the full Breit–Rabi Hamiltonian because the spectral simulation fully accounts for these effects. It is difficult to understand the consistent increase in the β-deuterium line spacing seen in spectra obtained from DMPO-d_{11}-OOH (VI). The effect would appear to be dependent on the spin trap, degree of deuteration, and frequency. Finally, with the use of two-dimensional spectral-spatial imaging, the potential for free radical localization is demonstrated. This work establishes a precondition for the direct identification of free radicals in vivo. Spin trapping studies in vivo are now in progress.

(37) Rosen, G. M.; Halpern, H. J.; Brunsting, L. A.; Spencer, D. P.; Strauss, K. E.; Bowman, M. K.; Wechsler, A. S. *Proc. Natl. Acad. Sci. U.S.A.* **1988**, *85*, 7772.

(38) Hall, E. J. *Radiobiology for the Radiologist*, 3rd ed.; J. B. Lippincott: Philadelphia, PA, 1989; p 249.

(39) Halpern, H. J.; Bowman, M. K. Low-frequency electron paramagnetic resonance. In *EPR Imaging and In Vivo EPR*; Eaton, G., Eaton, S., Eds.; CRC Press: Orlando, FL, 1991; p 45.

Acknowledgment. This research was supported in part by grants from the NIH, CA-50679 and HL-33550, the Balaban Foundation, the Council for Tabacco Research-USA, Inc., and the NSF, The Chemistry of Life Sciences Program, DCB-8616115. We acknowledge the useful comments of Michael K. Bowman of the Argonne National Laboratory and the assistance of Becky Nyquist of the University of Chicago.

Supplementary Material Available: Description of calculations, tables of NMR data derived from the Breit-Rabi Hamiltonian equation for compounds IV-IX, and figures showing the low modulation amplitude spectra and spectral simulations of the superoxide adducts of compounds IV-VI and the hydroxyl adduct of compound IX (13 pages). Ordering information is given on any current masthead page.

Electronic Transition Moment Directions and Identification of Low-Energy $n\pi^*$ States in Weakly Perturbed Purine Chromophores

Bo Albinsson* and Bengt Nordén

Contribution from the Department of Physical Chemistry, Chalmers University of Technology, 412 96 Göteborg, Sweden. *Received April 6, 1992*

Abstract: Measurements of UV linear dichroism on purine and three methyl derivatives partially oriented in poly(vinyl alcohol) matrix gave direct evidence for the assignment of the first singlet $n\pi^*$ state. Intensity distributions and moment directions for the first three $\pi \rightarrow \pi^*$ transitions were also determined. The $\pi \rightarrow \pi^*$ transitions in purine were found to be polarized at (angles, relative to the pseudo-symmetry long axis, counted positive in the N7 direction): $-31° \pm 5°$ (II at 265 nm), $+38° \pm 5°$ (III at 244 nm), and $+36° \pm 10°$ (IV at 214 nm). The transition energies and moment directions were not markedly perturbed by methyl substitution at the sixth, seventh, or ninth position. Therefore, these methyl substituents could be used as *orientational* perturbers to resolve a sign ambiguity problem regarding transition moment directions. The orientation parameters were determined by infrared dichroic measurements using both in-plane and out-of-plane polarized vibrational transitions. In addition, the phosphorescence spectra were studied, including phosphorescence anisotropy, phosphorescence lifetimes, and quantum yields, for the purines in an organic glass at 80 K. Based on these measurements, the lowest triplet state is concluded to have effectively $\pi\pi^*$ character, and its emission allowedness appears to originate from spin-orbit interactions primarily with singlet $\sigma\pi^*$ states but also with singlet $\pi\pi^*$ states via vibronic mixing. The phosphorescence emission spectra of purine and 6-methylpurine are complex, compared to 7-methylpurine and 9-methylpurine, with emission wavelength-dependent lifetimes and excitation spectra. This is ascribed to a prototropic tautomeric equilibrium between the 7H and 9H forms of purine and 6-methylpurine, a ground-state heterogeneity that we believe has caused confusion in earlier studies and, e.g., led to an incorrect assignment of the phosphorescence origin of purine.

Introduction

Excited-state properties of the purine chromophore are of utmost importance for understanding the spectroscopy of nucleic acids. Many questions are still to be resolved such as those concerning the unexpected low emission yields of the DNA bases and the potential influence of the $n\pi^*$ states. A number of investigations have been performed to understand the primary processes lowering the quantum yields for emission in the purine bases. The emerging picture is that very fast internal conversion ($k_{ic} = 10^{11}-10^{12}$ s^{-1}) efficiently competes with the radiative processes even at liquid nitrogen temperature,[1,2] but no detailed description of the quenching process has so far been given. The energy order of the excited states of the purine chromophore is very sensitive to electron-donating substituents at certain positions, which makes the emission properties highly sensitive in this respect. Near degeneracy of the $n\pi^*$ and $\pi\pi^*$ states has been proposed to increase internal conversion in N-heterocyclic systems,[3,4] and, thus, a detailed knowledge of the lowest excited states would be expected to become a key parameter to understand the photophysics of the purine bases.

Purine is a logical model chromophore for the nucleic acid bases adenine and guanine. Theoretical correlation between the excited states of purine and the nucleic acid bases has been proposed by Hug and Tinoco.[5] They calculated the transition monopoles and used the nodal properties of the wave functions to identify and characterize the different electronic transitions. Callis has extended their approach to include off-diagonal terms in the transition density matrix[6,7] and thereby found large similarities between adenine and purine, but not between guanine and purine, for the two lowest $\pi \rightarrow \pi^*$ transitions. In spite of the key roll of purine in various contexts, only a few experimental studies have been reported. Cohen and Goodman from phosphorescence and polarized phosphorescence spectra on purine made an indirect $n\pi^*$ assignment of the lowest excited state.[8] Drobnik et al. addressed several important questions on the solvent and substitution sensitivity of the purine electronic states.[9-12] They found evidence for an $n\pi^*$ state to be lowest in energy and argued for two $\pi \rightarrow \pi^*$ transitions in the 260-nm band. Chen and Clark performed a polarized reflection study on purine crystals[13] and calculated

(1) Eisinger, J.; Lamola, A. A. In *Excited States of Proteins and Nucleic Acids*; Steiner, R. F., Weinryb, I., Eds.; Plenum Press: New York, 1971.
(2) Callis, P. R. *Annu. Rev. Phys. Chem.* **1983**, *34*, 329-357.
(3) Lim, E. C. *J. Phys. Chem.* **1986**, *90*, 6770-6777.
(4) Wassan, W. A.; Lim, E. C. *Chem. Phys.* **1980**, *48*, 299-305.
(5) Hug, W.; Tinoco, I., Jr. *J. Am. Chem. Soc.* **1973**, *95*, 2803-2813.
(6) Callis, P. R. *Photochem. Photobiol.* **1986**, *44*, 315-332.
(7) Callis, P. R. *Int. J. Quantum Chem., Quantum Chem. Symp.* **1984**, *18*, 579-588.
(8) Cohen, B. J.; Goodman, L. *J. Am. Chem. Soc.* **1965**, *87*, 5487-5490.
(9) Drobnik, J.; Augenstein, L. *Photochem. Photobiol.* **1966**, *5*, 13-30.
(10) Drobnik, J.; Augenstein, L. *Photochem. Photobiol.* **1966**, *5*, 83-97.
(11) Kleinwächter, V.; Drobnik, J.; Augenstein, L. *Photochem. Photobiol.* **1967**, *6*, 133-146.
(12) Drobnik, J.; Kleinwächter, V.; Augenstein, L. *Photochem. Photobiol.* **1967**, *6*, 147-154.
(13) Chen, H. H.; Clark, L. B. *J. Chem. Phys.* **1969**, *51*, 1862-1871.

0002-7863/93/1515-223$04.00/0